ELSEVIER

Journal of Alloys and Compounds 330–332 (2002) 280–286

Journal of ALLOYS AND COMPOUNDS

www.elsevier.com/locate/jallcom

ZrNi–H_2: microstructural analysis of the thermodynamically controlled hydride phase growth, and electronic properties

N. Michel, S. Poulat, P. Millet, P. Dantzer*, L. Priester, M. Gupta

CNRS-UMR 8647, bât 415, Université Paris Sud, 91405 Orsay Cedex, France

Abstract

The ZrNi–H_2 phase diagram indicates the presence of two stable hydrides: a triclinic monohydride ZrNiH and an orthorhombic trihydride $ZrNiH_3$ [1]. In this paper, we present the results of some thermodynamic, microstructural and electronic properties of the ZrNi–H_2 system. A strict control of the thermodynamic variables (*P*, *T*) during the hydride phase growth allowed us to prepare two samples of overall composition $ZrNiH_{0.70}$ and $ZrNiH_{2.5}$. In a first step, the microstructure evolutions induced by hydrogen absorption are investigated during the activation process. The intermetallic and hydrided compounds are studied by energy dispersive X-ray spectroscopy (EDXS) and X-ray diffraction (XRD) methods. The nature of defects generated in ZrNi and its hydrides compounds are observed by transmission electron microscopy (TEM) and scanning electron microscopy (SEM). Ab-initio electronic structure calculations have been performed. They clearly show the importance of chemical effects besides geometrical factors in explaining the preferential site occupancy of hydrogen atoms in the ZrNiH phase.

Keywords: ZrNiH; $ZrNiH_3$; Hydride phase growth; Microstructure; Electronic properties

1. Introduction

The ZrNi was the first intermetallic compound investigated for its hydrogen storage properties [2]. The structural characterization was determined by Westlake et al. [3]. Since the earlier reports, the most extensive thermodynamic studies were carried out by Luo et al. [4]. Recently, the temperature dependence of the relative enthalpy of transformation for the β to γ formation of $ZrNiH_{3-\delta}$ was determined by heat flux calorimetry [5] and was analyzed by Dantzer et al. [6]. In the first part of the paper, we report our investigation of the chemical and microstructural properties of three compounds, the pure intermetallic and two hydrided compounds. These observations allow us to follow the morphological microstructure induced by hydrogen absorption during the activation process. Such microstructural studies are performed for the first time on samples prepared under controlled isothermal thermodynamic conditions.

In the ZrNi–H_2 system, it is remarkable that the Zr_4 (4*c*) sites that are occupied in ZrNiH become empty in the trihydride in favor of the pyramidal Zr_3Ni_2 (4*c*) and tetrahedral Zr_3Ni (8*f*) sites. This is a very unusual feature among hydrides. Therefore an interesting problem is to examine why the Zr_3Ni_2 (4*c*) sites, which satisfy the geometrical criteria of minimum hole size and minimum H–H distances [3] do not get filled first in the monohydride. The results of our ab-initio electronic band structure calculations are used to discuss this question.

2. Hydride phase growth

The main problem in the thermodynamic characterization and preparation of hydrides is to maintain the isothermal conditions at the sample level during the transformation. It is mainly due to the presence of a powdered material of low thermal conductivity and the presence of hysteresis. If isothermal conditions are not met, the thermodynamic path followed by the transformation is affected by the different possibilities of coupling between hysteresis, temperature gradients and concentration gradients. To fulfill isothermal conditions, and to insure homogeneous growth of the sample, the main parameters to be controlled are the gas flow coupled with a strict control of temperature variation inside the sample. This was achieved with the equipment specifically developed for the thermodynamic characterization of hydrides [5]. Thus, during hydride growth, 'quasi-isothermal' conditions

*Corresponding author.

E-mail address: pierre.dantzer@lemhe.u-psud.fr (P. Dantzer).

0925-8388/02/$ – see front matter
PII: S0925-8388(01)01651-6

were obtained with an accepted maximum temperature rise of 0.5°C at the sample level. Accordingly, the hydrogen flow rate did not pass beyond 1 μmol $H.s^{-1}$. Hydriding was performed at 85°C for the preparation of samples of overall composition $H/M=0.72_9$ (sample 1) and $H/M=2.50_0$ (sample 2). According to the thermodynamic studies [4,6], sample 1 corresponds to the presence of the monohydride phase in the α+β domain, while sample 2 corresponds to the non-stoichiometric trihydride phase, close to the end of the β+γ domain. The hydride samples were prepared during the activation process. Note that due to the soft activation, sample 1 (α+β phases) kept its original bulk morphology, sample 2 (β+γ phases) was reduced into powder.

3. Structural and chemical characterizations

3.1. Experimental techniques

The structure of the intermetallic and hydrided compounds is analyzed by X-ray diffraction technique (XRD). The $\Theta-2\Theta$ spectra are recorded from 10° to 90° with 0.02°/step and 7 s count/step and using the Cu Kα radiation.

The microstructure of these three compounds is performed by scanning electron microscopy (SEM) and by transmission electron microscopy (TEM). The TEM specimens are prepared by mechanical polishing, using the tripod polishing technique. To obtain the electron transparency, this technique was combined with ion milling (PIPS) for ZrNi and monohydride compounds. The dislocation Burger vectors $\vec{b}$ were determined using the invisibility criterion $\vec{g}\cdot\vec{b}=0$ [7]. The dislocation lines $\vec{u}$ were deduced from the orientation of their projection in three non-coplanar planes. The glide plane is given by $\vec{b}\times\vec{u}$.

The chemistry of the samples is studied in the scanning electron microscope equipped with a microprobe for energy dispersive X-ray spectroscopy (EDXS) and by Castaing microprobe.

3.2. Results and discussion

3.2.1. ZrNi

Castaing microprobe analyses lead to a composition of $Zr_{1.0043}Ni_{0.9957}$. The least squares refined lattice parameters, obtained from EDX patterns, are compatible with an orthorhombic unit cell with lattice parameters $a=0.325_9$ nm, $b=0.994_7$ nm and $c=0.408_8$ nm. These values well agree with the previously published data [8].

The starting material contains a high density of defects. Twins are homogeneously distributed in the matrix (Fig. 1). They are characterized by the following twinning planes: {110} and {021}. Dislocations with a mixed character are also observed with a Burger vector $\vec{b}=[100]$ and a line $\vec{u}=[121]$. The glide plane is (012). This TEM micrograph also shows the presence of a secondary phase of composition $Zr_{8.964}Ni_{11.036}$, which lies along the grain boundaries of the matrix.

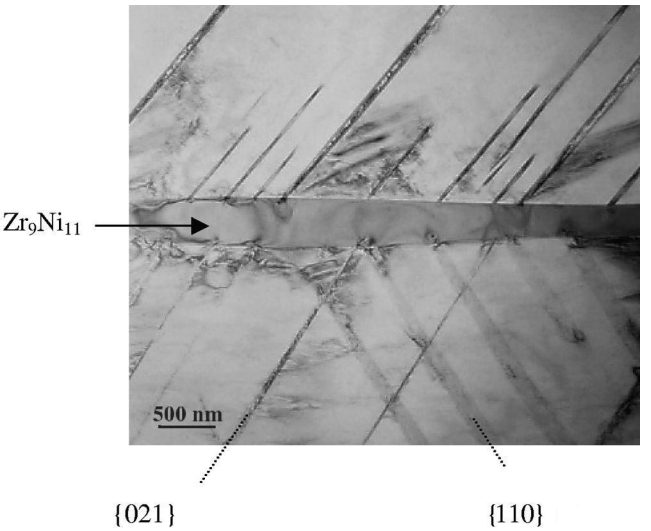

Fig. 1. TEM micrograph showing twins distributed in the matrix, and the presence of Zr_9Ni_{11} lying along the grain boundaries of the matrix.

3.2.2. $ZrNiH_{0.729}$

The EDXS, SEM and XRD experiments indicate the polycrystalline character of the hydrided sample. The three following phases are present: ZrNiH, ZrNi, and Zr_9Ni_{11}. The XRD pattern gives, for the triclinic monohydride phase, the following parameters: $a=0.333_0$ nm, $b=1.018_3$ nm and $c=0.403_4$ nm and $\alpha=89.18°$, $\beta=89.6°$ and $\gamma=89.43°$, in agreement with previous reports [9].

The SEM micrograph, in Fig. 2, shows grains with a high density of microcracks and other grains free of them. These microcracks are not observed in the starting material and are certainly associated with the presence of hydrogen. It can be noted that the Zr_9Ni_{11} phase is also free of microcracks, meaning that the secondary phase does not play a role in the hydrogen absorption under the conditions of preparation.

The TEM observations show that the ZrNiH phase precipitates with a plate like morphology in the ZrNi matrix. The coexistence of the intermetallic and the hydrided phase is in agreement with thermodynamic preparation condition. Depending on the ZrNi grain orientation two types of precipitates are observed. In one case, they appear as clusters surrounded by many dislocations seen in Fig. 3. This high density of dislocations does not allow the defect characterization. In the other case, the monohydride precipitates appear as fine platelets arranged in parallel ribbons (Fig. 4). They are also associated with numerous dislocations. The volume expansion during the

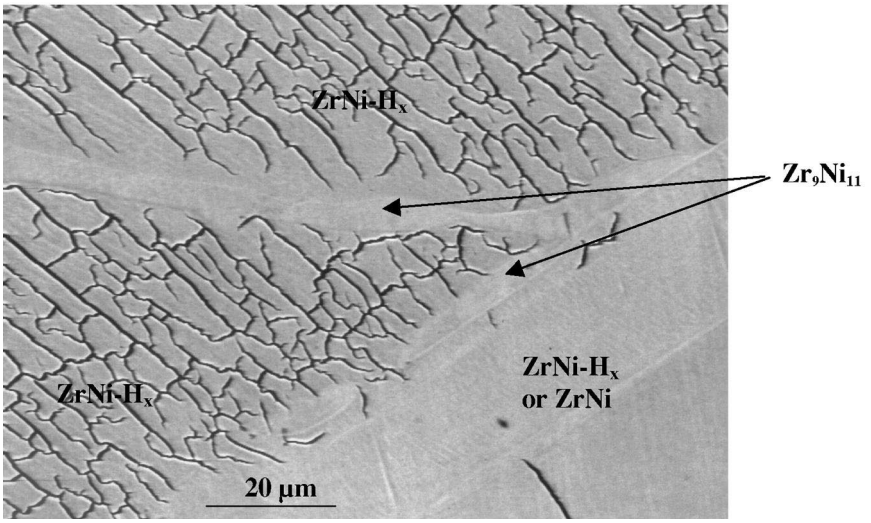

Fig. 2. SEM micrograph: grains with a high density of microcracks and other grains free of cracks. Zr_9Ni_{11} phase is free of cracks.

formation of hydride can explain these dislocations generation.

3.2.3. $ZrNiH_{2.500}$

The trihydride is pulverulent. The powder granules are polycrystalline and polyphase. The EDXS experiment still reveals the presence of the Zr_9Ni_{11} phase (Fig. 5). The light gray contrast observed on the SEM micrograph of a polished grain could correspond either to another phase or to grains with different orientations with respect to the matrix. As the EDXS analyzer cannot detect hydrogen, the ambiguity is not resolved. The XRD pattern displays the peaks characterizing the $ZrNiH_{3-\delta}$ compound. This compound presents an orthorhombic structure [10] with lattice parameters $a = 0.352_8$ nm, $b = 1.046_4$ nm, $c = 0.428_6$ nm. Due to the overall composition of sample 2, $H/M = 2.50_0$, and the sensitivity of the XRD, it is not surprising that the presence of small amount of ZrNiH below 5% can not be detected.

The TEM micrograph (Fig. 6) of a powder granule shows large and small bands, which seem to be related to the coexistence of the ZrNiH and $ZrNiH_{3-\delta}$ phases. Indeed, the electron diffraction pattern corresponding to

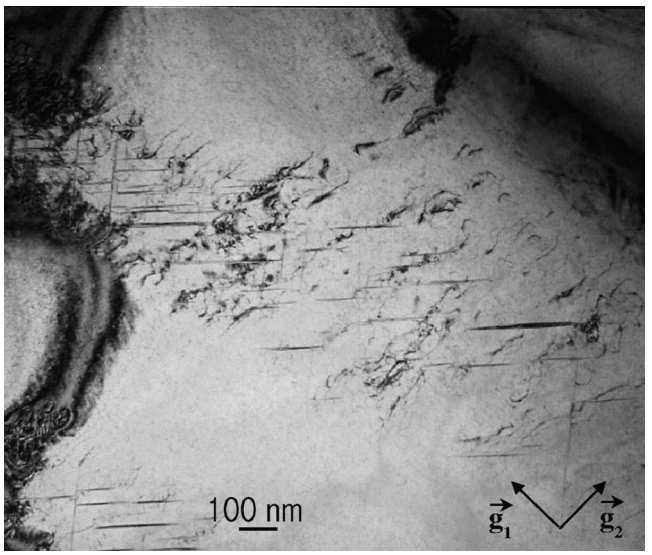

Fig. 3. Bright field micrograph taken with $\vec{g}_2$: plate like clusters precipitates of ZrNiH phase ($\vec{g}_1 = [010]$ and $\vec{g}_2 = [001]$ indicate the sample orientation).

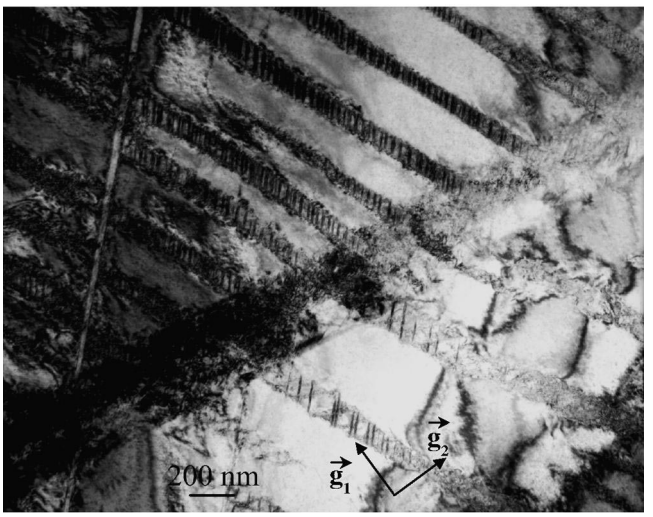

Fig. 4. TEM micrograph: ZrNiH precipitates appearing in an ordered way forming parallel bands ($\vec{g}_1 = [001]$ and $\vec{g}_2 = [130]$ indicate the sample orientation).

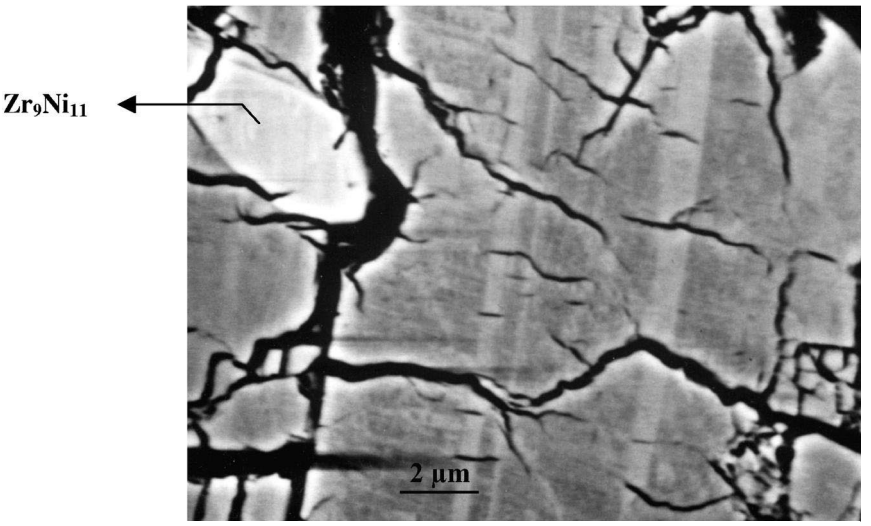

Fig. 5. SEM micrograph of a polished powder granule with Zr_9Ni_{11} phase; the light gray contrast corresponds either to another phase or to grains with different orientations with respect to the matrix.

this image gives the following orientation relationships between these two compounds:

$$[121]_{ZrNiH}//[411]_{ZrNiH_{3-\delta}}$$
$$(2\bar{1}0)_{ZrNiH}//(1\bar{5}\bar{1})_{ZrNiH_{3-\delta}}$$

The contrast of the bend contours can be associated to a high density of dislocations. Further analyses are in progress to verify this assumption.

Our results can be compared with those of Kronski et al. [1] who electrolytically charged pre-thinned samples for TEM. From their analyses they report long plate-like β-precipitates and small metastable γ phase platelets in α-ZrNi. No orientation relationship between β and γ phase was given due to the difficulty of preparing a (β+γ) phase sample for TEM observations. A thermodynamic control of the hydride growth seems to be more suited to proceed with a microstructural analysis.

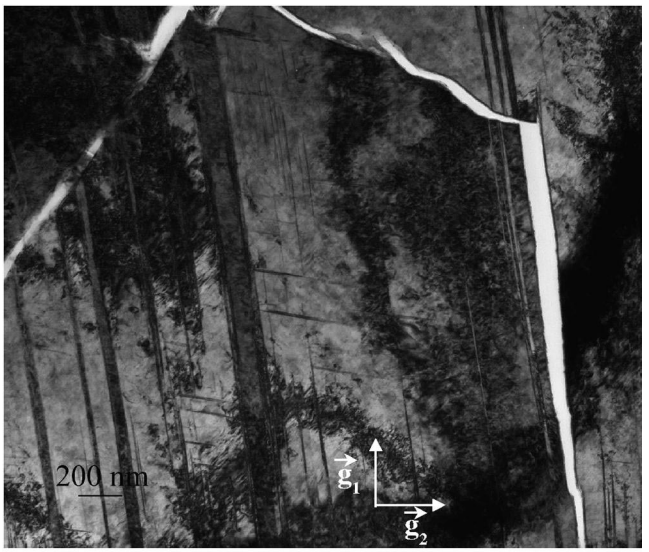

Fig. 6. TEM micrograph: platelet precipitates of $ZrNiH_{3-\delta}$ in ZrNiH ($\vec{g}_1$=[131] and $\vec{g}_2$=[241] indicate the sample orientation).

4. Electronic structure

The band structure calculations have been performed using the density functional theory (DFT) in the local density approximation (LDA) with the Van Barth–Hedin approach of the exchange and correlation potential. We have used the self-consistent linear muffin-tin orbital (LMTO) method within the atomic sphere approximation (ASA). We included the combined correction terms to account for the overlap of the atomic spheres. The densities of state (DOS) have been calculated with the linear energy tetrahedron method using a 1 mRy mesh.

The electronic structure of ZrNiH (D) was studied using the structural data obtained by neutron diffraction on the deuteride [11] in the *CmCm* symmetry, an assumption which is justified since the observed triclinic distortion is small.

We have performed two sets of electronic structure calculations corresponding to different site occupancies for the hydrogen atom in ZrNiH, one in which the hydrogen atoms occupy the Zr_4 (4*c*) sites as observed experimentally in the monohydride [12], and a second one in which the H atoms occupy the Zr_3Ni_2 (4*c*) sites which are filled in the

trihydride phase. The two types of sites satisfy the geometrical criteria of minimum hole size and minimum H–H distances as shown by Westlake [4].

The corresponding total densities of states and their projections around the different atomic sites are plotted respectively in Figs. 7 and 8. We shall first analyze the results of the experimentally observed phase ZrNiH. In Fig. 7, the structure of 2.6 eV width observed in the DOS at low energy correspond to one metal–hydrogen band per formula unit. The site analysis reveals clearly that the hydrogen metal interaction is largely dominated by the H–Zr bonding while the H–Ni interaction is much weaker.

At higher energies, the next structure observed in the DOS of the occupied states, of total width 3.9 eV,

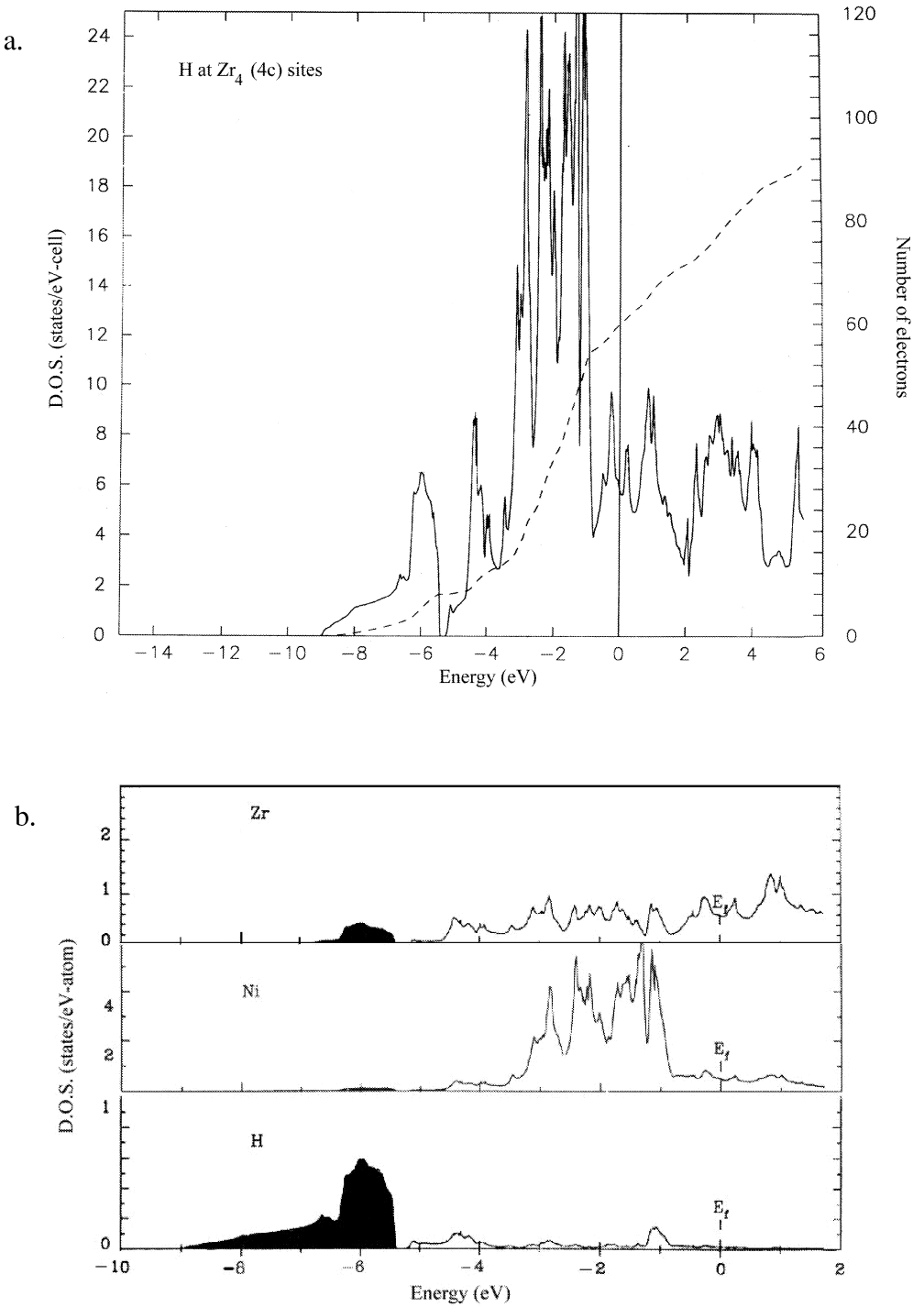

Fig. 7. (a) Total DOS of ZrNiH (full line) and number of electrons (dotted line). The hydrogen atoms occupy the Zr_4 (4c) sites. E_F is the origin of energies. (b) Projection around the different atomic sites. The metal–hydrogen bonding states are shaded.

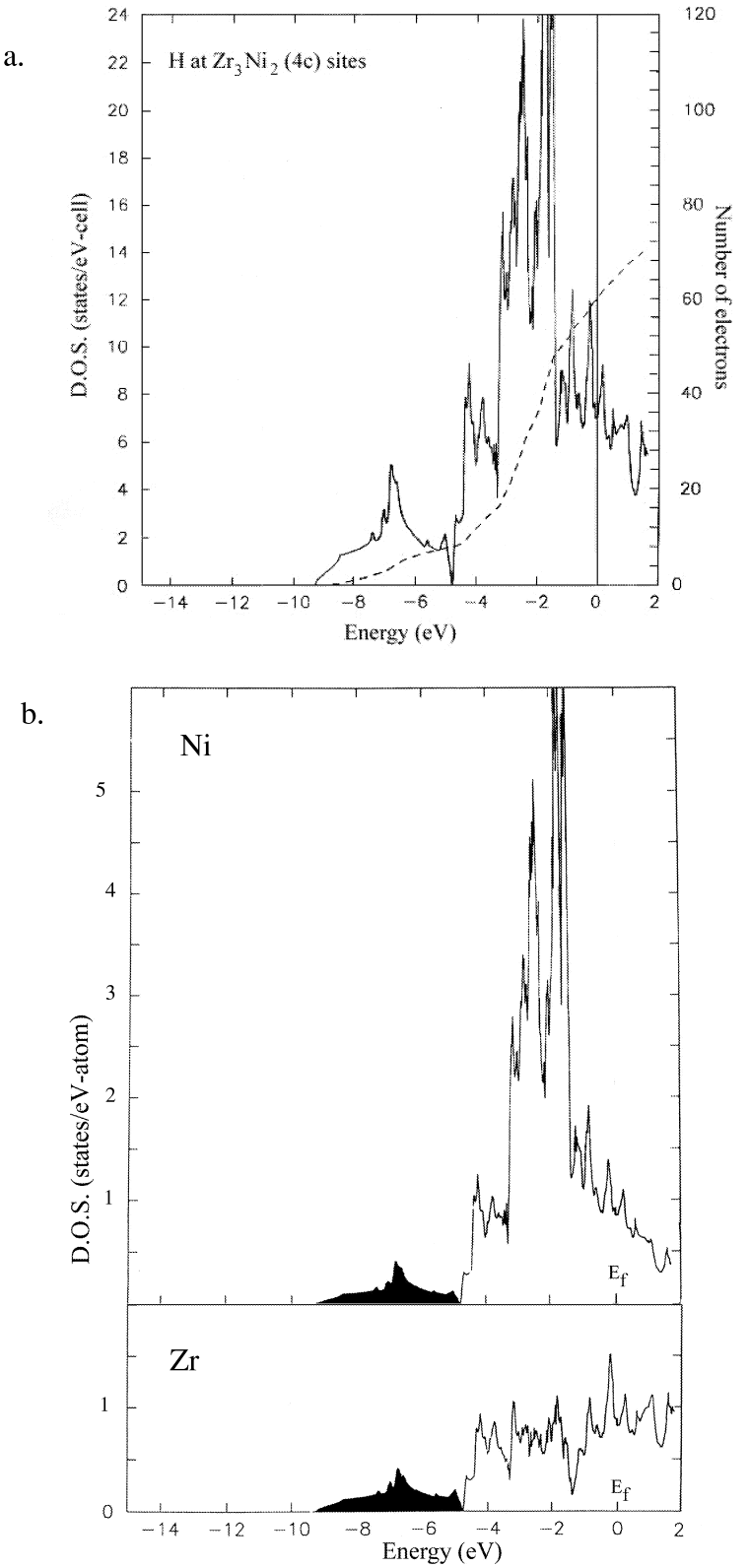

Fig. 8. (a) Total DOS of ZrNiH (full line) and number of electrons (dotted line). The hydrogen atoms occupy the Zr_3Ni_2 (4*c*) sites. E_F is the origin of energies. (b) Projection around the different atomic sites. The metal states contributing to the metal–H bonding are shaded.

corresponds mostly to the narrow, high DOS of the Ni 3d localized states. The mixing of the Zr 4d with the Ni 3d states is strong in this energy range. The Zr states are more delocalized and result in much broader bands of lower DOS. The metal d bands are hybridized with Zr and Ni s–p states. In ZrNiH, the Fermi energy, E_F, fall around 0.8 eV above the top of the Ni d bands. The Zr-d contribution at E_F is larger than that of the Ni-d states.

As shown in Fig. 8, the occupancy of the pyramidal Zr_3Ni_2 (4*c*) sites by hydrogen results in a drastic modification in the chemical nature of the metal-hydrogen interactions. The site analysis of the DOS shows clearly that in this case, the Ni and Zr contribution to the binding with hydrogen between 9.5 and 4.5 eV below E_F are comparable. The total energy is found to be 9 mRy higher than in the calculation reported in Fig. 7, in agreement with the experimental observation [11], which shows that the Zr_4 (4*c*) sites are occupied in the monohydride phase.

In order to understand the origin of the greater stability of the Zr_4 (4*c*) vs. Zr_3Ni_2 (4*c*) site occupancy, it is important to point out that the Ni-d, s, p states which participate in the metal–H bonding were already occupied in the pure intermetallic [13]; they are simply lowered in energy by the Ni–H interaction. The H–Zr interaction is crucial to the stability of the compound because it is strong enough to pull additional Zr-d states, empty in the intermetallic, below the Fermi level of the hydride. In this connection, a comparison of Figs. 7 and 8 shows that Zr_4 (4*c*) site occupancy leads to a lowering of E_F, the Fermi level is closer to the top of the Ni-d states. Moreover, since the Zr-4d states are higher in energy than the Ni-3d bands, the energy gain resulting from their lowering by the metal–hydrogen interaction is larger.

Thus, our calculations show clearly that the greater stability of the tetrahedral Zr_4 (4*c*) vs. the pyramidal Zr_3Ni_2 (4*c*) sites in ZrNiH is explained by chemical effects associated with the Zr–H interactions. At higher hydrogen concentrations, it is the repulsive H–H interaction at short distances, which leads to the observed H site occupancy in the $ZrNiH_3$ phase.

5. Conclusions

The microstructure evolution induced by hydrogen absorption for samples prepared under controlled isothermal thermodynamic conditions has been observed for the first time. The monohydride and trihydride phases appear as plate-like precipitates. It seems that the accommodation of stress generated by the precipitation are different depending on the hydrogen concentration: the ZrNiH precipitates are surrounded by numerous dislocations, while $ZrNiH_{3-\delta}$ precipitates are associated with cracks.

Work is in progress to explain, for the monohydride sample, why some grains contain microcracks while others are free of them, to determine the relation between cracks observed by SEM and precipitate clusters and ribbons observed by TEM and finally to emphasize the orientation relationships between the ZrNiH precipitates and the intermetallic ZrNi matrix.

The ab-initio electronic structure calculations performed for different interstitial site occupancies of the H atoms show that besides geometrical factors such as hole size and minimum H–H distances, the chemical effects associated mainly with the Zr–H interactions are crucial in explaining the stability and preferential H site occupancy in the ZrNiH phase.

Acknowledgements

Dr R.C. Bowman Jr. (JPL, CA, USA) is gratefully acknowledged for providing the ZrNi sample of high purity. We thank the IDRIS (Institut de Développement de Recherche en Informatique Scientifique) of CNRS (Centre National de la Recherche Scientifique) for providing us with the computing facilities used in the present work.

References

[1] R. Kronski, T. Schober, J. Alloys Comp. 205 (1994) 175.
[2] G.G. Libowitz, H.F. Hayes, T.R.P. Gibbs Jr., J. Phys. Chem. 62 (1958) 76.
[3] D.G. Westlake, J. Less-Common Met. 75 (1980) 177.
[4] W. Luo, A. Craft, T. Kuji, H.S. Chung, T.B. Flanagan, J. Less-Common Met. 162 (1990) 251.
[5] P. Dantzer, P. Millet, Rev. Sci. Instrum. 71 (2000) 142.
[6] P. Dantzer, P. Millet, T. Flanagan, Met. Mat. Trans. 32A (2001) 29.
[7] A. Howie, M.J. Whelan, Proc. R. Soc. A 267 (1962) 206.
[8] M.E. Kirkpatrick, D.M. Bailey, J.F. Smith, Acta Cryst. 15 (1962) 252;
M.E. Kirkpatrick, J.F. Smith, W.L. Larsen, Acta Cryst. 15 (1962) 894.
[9] I.E. Nemirovskaya, V.V. Lunin, J. Alloys Comp. 209 (1994) 93.
[10] A.V. Irodova, V.A. Somenkov, S.Sh. Shil'shtein, L.N. Padurets, A.A. Chertkov, Sov. Phys. Crystallogr. 23 (5) (1993) 591.
[11] D.G. Westlake, H. Shaked, P.R. Mason, B.R. Mac Cart, M.H. Mueller, J. Less-Common Met. 88 (1982) 17.
[12] S. Yang, F. Aubertin, P. Rehbein, U. Gonser, Zeits. Für Kristal. 195 (1991) 281.
[13] M. Gupta, J. Alloys Comp. 293–295 (1999) 190.